TASK QUARTERLY 8 No 3 (2004), 393–412

THE STRUCTURE OF RAREFIED AND DENSIFIED $PbSiO_3$ GLASS: A MOLECULAR DYNAMICS STUDY

GRZEGORZ BERGMAŃSKI[1], MICHAŁ BIAŁOSKÓRSKI[1,2], MONIKA RYCHCIK-LEYK[1], AGNIESZKA WITKOWSKA[1,2], JAROSŁAW RYBICKI[1,2], GIORGIO MANCINI[3], SANDRO FRIGIO[3] AND SANDRO FELIZIANI[3]

[1] *Department of Solid State Physics, Faculty of Technical Physics and Applied Mathematics, Gdansk University of Technology, Narutowicza 11/12, 80-952 Gdansk, Poland* {*tuptus, skorka, monika, agnieszk, ryba*}*@task.gda.pl*

[2] *TASK Computer Centre, Gdansk University of Technology, Narutowicza 11/12, 80-952 Gdansk, Poland*

[3] *Istituto di Matematica e Informatica, Università di Camerino, Madonna delle Carceri, 62-032 Camerino (MC), Italy* {*giorgio.mancini, sandro.frigio, sandro.feliziani*}*@unicam.it*

(Received 13 February 2004)

Abstract: The paper is a molecular dynamics (MD) study of the structure of rarefied and densified lead-silicate glass of the $PbSiO_3$ composition. Simulations have been performed in the constant volume regime for systems with densities of 3 000, 4 000, 5 000, 5 970 (normal density), 7 000 and 8 000 kg/m^3, using a two-body potential (Born-Mayer repulsive forces and Coulomb forces due to full ionic charges). All the systems were initially prepared as well equilibrated hot melts, and then slowly cooled down to 300 K. The information on short-range correlations was obtained in a conventional way (from radial and angular distribution functions), while the middle-range order was studied via cation-anion ring analysis, using our new programme for basal ring determination. The structure of rarefied and densified glasses is compared with the structure of the same glasses under normal conditions. Moreover, the present results on $PbSiO_3$ glass are compared with the corresponding data previously obtained for rarefied and densified $PbGeO_3$ glass (Rybicki *et al.* 2001 *Comput. Met. Sci. Tech.* **7** 91–112).

Keywords: oxide glasses, structure of glasses, ring analysis, MD simulations

1. Introduction

Lead-silicate glasses have found many industrial applications, mainly as optical glasses [1]. They are also used as special materials in electronics and optoelectronics

(in the production of image plate amplifiers and scintillators [2]). Modified lead-silicate glasses, containing metallic Pb granules, exhibit a high secondary emission coefficient, and thus find an application in the production of electron channel multipliers [3].

The atomic structure of lead-silicate glasses, $x\mathrm{PbO}(1-x)\mathrm{SiO}_2$, has been investigated for sixty years. Various experimental techniques have been used, such as IR spectroscopy [4], Raman spectroscopy [4–6], NMR [5, 7, 8], XPS [9], X-ray diffraction [10, 11], neutron diffraction methods [12, 13], EXAFS (Extended X-ray Absorption Fine Structure) and XANES (X-ray Absorption Near-Edge Structure) [7, 8, 14–17]. Also extensive molecular dynamics (MD) simulations were performed in the whole range of glass-formation ($0.1 \leq x \leq 0.9$) [17–23].

It is well known that most glasses, depending on the method of preparation, can have various densities with the same composition. In this respect, silica is probably the most studied material (*e.g.* [24–36]). Studies on low- and high-density forms of many binary silica glasses have also been performed. However, the atomic structure of rarefied [37] and densified silica glasses containing heavy-metal oxides, as far as the authors know have not been studied until now, neither experimentally, nor theoretically.

The present contribution is a molecular dynamics (MD) [38, 39] study of the structure of rarefied and densified lead-silicate glass of the PbSiO_3 composition. In order to see more clearly the structural features characteristic of low- and high-density states we have performed our simulations in a wide range of densities, from $3\,000\,\mathrm{kg/m^3}$ to $8\,000\,\mathrm{kg/m^3}$. As no experimental data on the atomic-level structure of low- or high-density states of the considered glasses are known, our MD results are predictive in character. However, the potential used in our simulations has recently been successfully applied in an extensive MD study of $x\mathrm{PbO}(1-x)\mathrm{SiO}_2$ glasses in a wide range of compositions at normal densities [17, 20–23], giving very good agreement with the available experimental data (see Appendix A). Thus, we have used the same potential for further MD studies in the belief that it reproduces equally well the structure of rarefied and densified glasses.

The paper is organised as follows. In Section 2, we describe the applied simulation technique and the methods of data analysis. The simulation results are described and discussed in Sections 3 and 4, where we describe in detail the short-range, and the medium-range order, respectively. In Section 5, we summarise the presented results on PbSiO_3 glasses, and compare them with similar results previously obtained for PbGeO_3. Section 6 contains our conclusions.

2. Simulation technique and methods of data analysis

2.1. MD runs

Our molecular dynamics simulations were performed in the constant volume regime (an NVE ensemble). The atoms were assumed to interact by the two-body Born-Mayer-Huggins potential:

$$V_{ij}(r) = \frac{q_i q_j}{4\pi\varepsilon_0 r} + A_{ij}\exp((\sigma_{ij}-r)/b_{ij}), \tag{1}$$

containing the Born-Mayer repulsive contribution, and Coulomb interactions, calculated using the standard Ewald technique. The potential parameters A_{ij}, b_{ij} and

σ_{ij}, taken from [18], were previously successfully applied in (NpT) simulations of $x\mathrm{PbO}(1-x)\mathrm{SiO}_2$ glasses for $0.1 \leq x \leq 0.9$ [17, 20–23]. We used full ionic charges. The number of atoms within the cubic simulation box with the usual periodic boundary conditions was equal to 2500. Depending on the density, the edge of the simulation box varied from about 30 to about 45 Å. We simulated $PbSiO_3$ glass with constant densities equal to 3 000, 4 000, 5 000, 5 970, 7 000, and 8 000 kg/m^3. The samples were initially prepared in a well-equilibrated molten state at 10 000 K, and then slowly cooled down to 300 K, passing equilibrium states at 8 000 K, 6 000 K, 5 000 K, 4 000 K, 3 000 K, 2 500 K, 2 000 K, 1 500 K, 1 000 K and 600 K. Temperature scaling was applied whenever the rolling average of temperature (calculated over last 100 time steps) went out from the interval $(T-\Delta T, T+\Delta T)$. At each intermediate temperature, the system was equilibrated during 30 000 fs time steps, using $\Delta T = 100$ K for $T \geq 1\,000$ K, $\Delta T = 20$ K for $T = 600$ K, and $\Delta T = 10$ K for $T = 300$ K. Equilibrated systems were sampled during 10 000 fs time steps. Such a run scheme corresponds to the average cooling rate of $2 \cdot 10^{13}$ K/s.

The resulting low- and normal-density structures ($3\,000\,\mathrm{kg/m^3} \leq \rho \leq 5\,970\,\mathrm{kg/m^3}$) turned out to be stable: the final 300 K-configurations were relaxed at zero external pressure conditions throughout 50 000 time steps, and the volumes of the systems changed only by several percent (5%–8%). Thus, the MD results obtained in this range of densities can be considered as 'true' (equilibrium) low-density glasses. Note that in [37] Ar-sputtered lead-silicate coatings of densities in the range from 3100 kg/m^3 to 4 000 kg/m^3 are reported. However, our MD-simulated densified structures were unstable: instead of slight volume relaxation we observed a continuous system expansion to normal density. Thus, the high-density MD data ($\rho > 5\,970\,\mathrm{kg/m^3}$) are considered here as corresponding to the $PbSiO_3$ glass under hydrostatic pressure rather than to stable high-density phases.

2.2. Structure recognition

Structural information on short-range correlations was obtained in a conventional way, mainly from radial and angular distribution functions (RDFs and ADFs, respectively). However, in order to describe the second and further co-ordination shells, *i.e.* the medium-range order, one should use more advanced methods of structural analysis than analysing the RDFs and ADFs. One of the possible approaches consists in the analysis of properly constructed clusters of edge- and/or face-sharing Voronoï polyhedra [40–42]. This method, although very efficient in the detection of crystalline regions of various symmetries [43] works well for close-packed systems only. In open systems serious problems appear in the construction of the Voronoï network and in the procedures eliminating short edges and small faces. In such cases, the cation-anion ring analysis seems to be an ideal tool for characterising the medium-range order. The medium-range order was studied mainly via cation-anion ring analysis, performed using a new and highly efficient redundancy-aware algorithm. Since the method is a novelty, we present its main guidelines in Appendix B. The structure of the determined basal rings was investigated using the ANELLI programme package [44–46].

3. Short-range order

Figure 1 shows the first Si–O, Pb–O and O–O peaks of radial distribution functions in $PbSiO_3$ glass for three various densities. Several angular distribution functions are shown in Figure 2. As can be seen in Figure 1, most of the first RDF peaks reveal a rather significant asymmetry. As it has been shown in a number of papers, RDFs in disordered systems can be decomposed in a short-range peak of a well-defined shape, and a long-range tail [47, 48]. A simple Gaussian shape of the short-range peak of RDF is usually insufficient to accurately describe the short-range ordering in highly disordered systems. A useful parameterisation of the first RDF peak, as shown in [48, 49], has the form:

$$g(r) = \frac{Np(r)}{4\pi\rho r^2}, \tag{2}$$

where N is the co-ordination number, ρ is density. The bond length probability density $p(r)$ is described by a Γ-like distribution. The corresponding formula, valid for $(r-R)\beta > -2\sigma$, reads as follows:

$$p(r) = \frac{2}{\sigma\cdot|\beta|\cdot\Gamma(4/\beta^2)}\cdot\left(\frac{4}{\beta^2}+\frac{2\cdot(r-R)}{\sigma\cdot\beta}\right)^{\frac{4}{\beta^2}-1}\cdot\exp\left[-\left(\frac{4}{\beta^2}+\frac{2\cdot(r-R)}{\sigma\cdot\beta}\right)\right]. \tag{3}$$

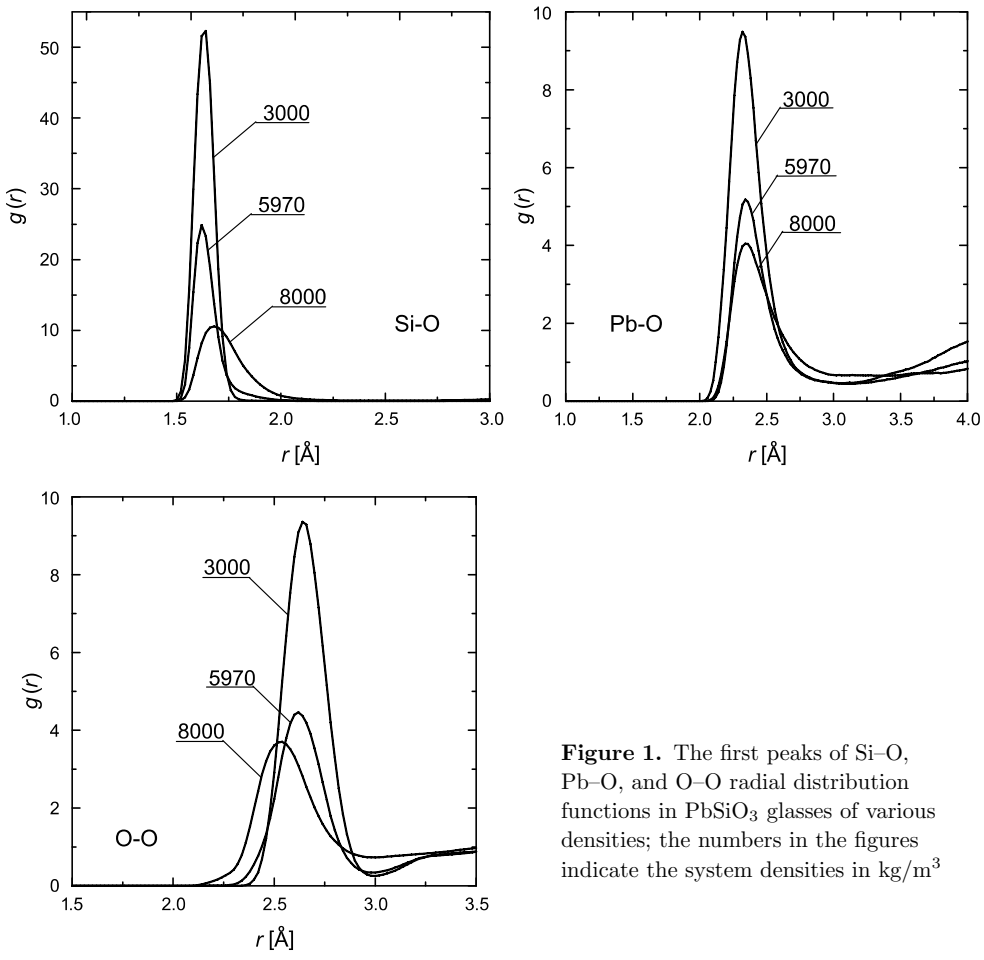

Figure 1. The first peaks of Si–O, Pb–O, and O–O radial distribution functions in $PbSiO_3$ glasses of various densities; the numbers in the figures indicate the system densities in kg/m^3

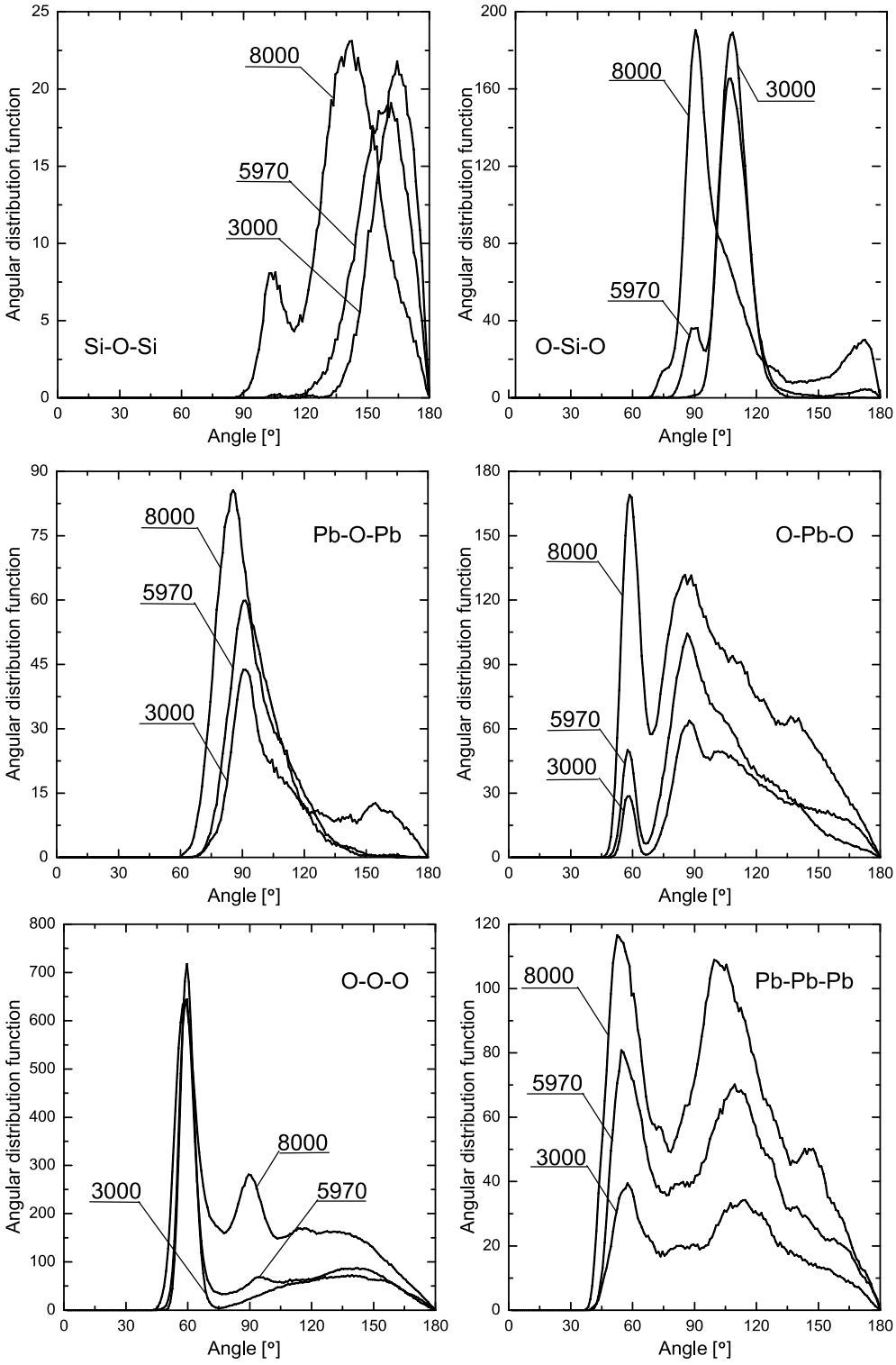

Figure 2. Selected angular distribution functions in $PbSiO_3$ glasses of various densities; the numbers in the figures indicate the system densities in kg/m^3

Here R is the average distance, σ^2 is variance (a Debye-Waller-like parameter), β is the asymmetry (skewness) parameter, and $\Gamma(x)$ is Euler's gamma function, calculated for $x = 4/\beta^2$. The best-fit parameters R, σ^2, β, and N are listed in Tables 1 and 4. The short-range ordering around the Si^{4+} and Pb^{2+} cations is described in Subsections 3.1 and 3.2, respectively.

3.1. Short-range order around silicon ions

3.1.1. Inter-atomic distances

In the density range from 3 000 kg/m^3 to 5 000 kg/m^3, the first Si–O peak can be excellently approximated by a single Γ-like function. The mean Si–O distance, R, is density-independent (1.64 Å), and the corresponding values of the Debye-Waller-like parameter, σ^2, and the skewness parameter β, are stable and very low in this range of density. Thus, in our MD-simulated glass the effective Si–O force field exhibits rather low anharmonicity in rarefied samples.

Table 1. The structural parameters R, σ^2, β and N for Si–O, O–O, and Pb–O first peaks of radial distribution functions in $PbSiO_3$ glasses of various densities

ρ	Si–O					O–O					Pb–O				
[kg/m^3]		R [Å]	σ^2 [Å^2]	β	N		R [Å]	σ^2 [Å^2]	β	N		R [Å]	σ^2 [Å^2]	β	N
3000	(I)	1.64	0.002	0.21	4.00	(I)	2.67	0.011	0.30	4.05	(I)	2.38	0.017	0.74	3.74
4000	(I)	1.64	0.002	0.20	4.02	(I)	2.67	0.011	0.29	4.05	(I)	2.38	0.018	0.71	3.68
5000	(I)	1.64	0.002	0.21	4.03	(I)	2.67	0.010	0.24	4.06	(I)	2.39	0.016	0.74	3.93
5970	(I)	1.64	0.002	0.53	3.72	(I)	2.68	0.012	0.80	3.70	(I)	2.42	0.021	0.92	4.41
	(II)	1.81	0.010	0.65	0.42	(II)	2.49	0.004	0.02	0.60					
7000	(I)	1.64	0.002	0.51	2.14	(I)	2.65	0.021	0.83	4.44	(I)	2.40	0.016	0.66	4.12
	(II)	1.76	0.012	0.68	2.36	(II)	2.46	0.010	0.01	0.55	(II)	2.76	0.040	0.76	1.61
8000	(I)	1.61	0.002	0.67	0.29	(I)	2.62	0.026	0.91	5.45	(I)	2.40	0.017	0.65	4.52
	(II)	1.76	0.012	1.05	4.64	(II)	2.37	0.013	0.10	0.40	(II)	2.75	0.037	0.76	2.14

At normal and higher densities, however, it is impossible to reproduce the first Si–O RDF peak with a single Γ-like function: the peaks split into two sub-shells (see Table 1). The first sub-peak (I) has parameters similar to those of the main peak in rarefied samples, but is significantly lower. The associated mean co-ordination number decreases from about 3.7 at normal density to 0.3 at 8 000 kg/m^3, which means that this sub-shell practically disappears in the highest-density sample. The second, more distant peak II, with R equal to about 1.8 Å, is wider and more asymmetric than sub-peak (I). The associated co-ordination number increases from 0.4 at normal density to about 4.6 at the highest density, so that the second sub-peak becomes dominant at high densities. The total co-ordination of the two sub-shells amounts to about 4.1, 4.5 and 5.0 at 5 970, 7 000 and 8 000 kg/m^3, respectively.

The mean O–O distance, R, is constant for rarefied glasses and equals 2.67 Å, and decreases by as little as 0.05 Å between 5 970 kg/m^3 and 8 000 kg/m^3 (see peak marked I in Table 1). The decrease in the O–O inter-atomic distances is accompanied by an increase in peak width and the degree of its asymmetry. The dispersion parameter, σ^2, of the O–O distances is much higher than that of the Si–O distances

(5–10 times). Simultaneously, the asymmetry degrees for the main Si–O and O–O peaks are similar. An increase of the σ^2 and β parameters with increasing density is accompanied by an increase of the average co-ordination number: from 4 for 3 000kg/m^3 to about 6 for 8 000kg/m^3. Starting from 5 970kg/m^3, the first O–O peak, like the Si–O peak, splits into two sub-peaks, shown in Table 1 as peaks I and II.

3.1.2. Structural unit

Using the data on inter-atomic distances listed in Table 1 and angular distributions from Figure 2, one can conclude that, for $\rho <$5 970kg/m^3, the basic structural units of the silica subsystem are SiO_4 tetrahedrons. A detailed analysis of the atom configurations has shown that, for densities up to 5 000kg/m^3, over 99% of Si atoms have a four-fold, tetrahedral oxygen co-ordination. However, at the densities of 5 970kg/m^3, 7 000kg/m^3 and 8 000kg/m^3, the fraction of tatrahedrally co-ordinated Si atoms is 87%, 61% and 32% (Table 2), respectively.

Table 2. The occurrence [%] of SiO_4, SiO_5 and SiO_6 groups at various glass densities

	SiO_4	SiO_5	SiO_6
3 000kg/m^3	99.6%	0.4%	—
4 000kg/m^3	100.0%	—	—
5 000kg/m^3	98.6%	1.4%	—
5 970kg/m^3	87.2%	12.8%	—
7 000kg/m^3	61.0%	36.4%	2.6%
8 000kg/m^3	32.4%	57.4%	10.2%

In order to characterise the SiO_4 tetrahedra we have introduced tetrahedricity parameters, T_1 [50] and T_2 [51]:

$$T_1 = \frac{\sum_i (l_{\mathrm{O-O},i} - l_{\mathrm{O-O}})^2}{l^2_{\mathrm{O-O}}}, \tag{4}$$

$$T_2 = \frac{\sum_i (l_{\mathrm{O-O},i} - l_{\mathrm{O-O}})^2}{l^2_{\mathrm{O-O}}} + \frac{\sum_i (l_{\mathrm{Si-O},i} - l_{\mathrm{Si-O}})^2}{l^2_{\mathrm{Si-O}}}, \tag{5}$$

where $l_{\mathrm{O-O},i}$ are the lengths of the i^{th} tetrahedrons' O–O edges, $l_{\mathrm{Si-O},i}$ are the Si–O distance, and $l_{\mathrm{O-O}}$ and $l_{\mathrm{Si-O}}$ are the average O–O and Si–O distances for the considered tetrahedron. The T_1 parameter estimates only the overall shape of the tetrahedra, with no reference to the position of the central cation. The newly-introduced shape estimator (5) additionally takes into account deviations in the cation's position. The ideal tetrahedron is characterised by zero values of both the T_1 and T_2 estimators. (For a detailed study of the dependence of distributions of the T_1 and T_2 values on the degree of tetrahedra deformation see [52]). In definitions (4) and (5) one could also use global (calculated over all the tetrahedral present in the simulation box) average O–O and Si–O distances. In the case of considered glasses, the distributions of the T_1 and T_2 values, calculated with both estimator definitions, are practically identical. We prefer using the cation-anion and anion-anion average distances calculated for individual tetrahedra, since such approach remains equally

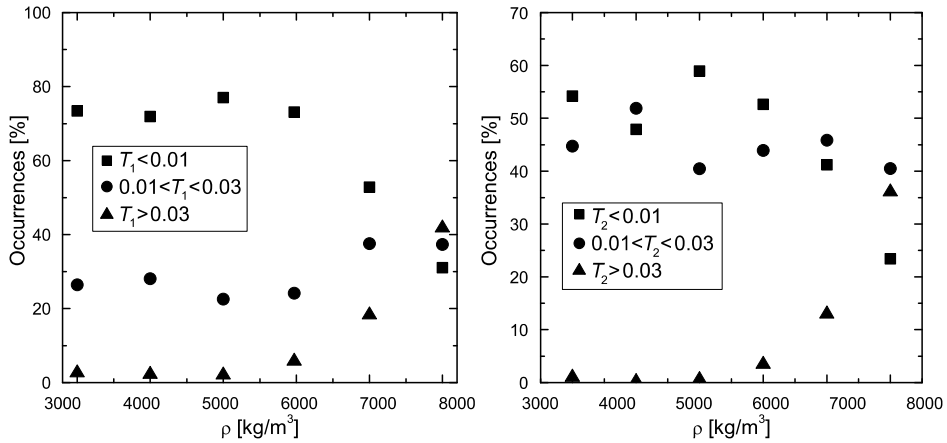

Figure 3. Density dependence of the T_1 and T_2 value distributions calculated for SiO_4 tetrahedra

correct in application to more complex systems, *e.g.* with coexisting SiO_4 and GeO_4 tetrahedra.

In the present simulations, the distributions of values of the tetrahedricity parameters T_1 and T_2 are similar for a given density ρ, and both vary in a function of ρ (Figure 3). The obtained distributions of the T_1 and T_2 parameter values for glass densities $\rho < 5\,970\,\mathrm{kg/m^3}$ correspond to the tetrahedra relative deformation degree[1] of about 2%–3%. Thus, SiO_4 units can be considered as vibrating regular tetrahedra. At the same time, the distributions of T_1 and T_2 parameter values obtained for densified samples correspond to relative deformation of 6%–10%. Thus, SiO_4 units in compressed samples show rather high degree of structural disorder.

As mentioned above, in the $5\,970\,\mathrm{kg/m^3}$, $7\,000\,\mathrm{kg/m^3}$, and $8\,000\,\mathrm{kg/m^3}$ glasses, 13%, 39% and 68% of all the Si atoms, respectively, have oxygen co-ordination other than 4 (Table 2). These are mainly SiO_5 groups (13%, 36% and 57% of all Si atoms, respectively). The SiO_5 groups obtained in our simulations may be one of two quite well defined structures: a square pyramid, with the Si atom close to the middle of the pyramid base (Figure 4c) or a triangular bi-pyramid (Figure 4e). The appearance of the peaks at 90° and 180° in high-density O–Si–O angular distributions (see Figure 2) is directly related to the geometry of theses SiO_5 structures. The occurrence frequency of the SiO_6 groups in densified samples (Table 2), all identified as distorted square bi-pyramids (Figure 4f), amounts to 3% and 10% at the densities of $7\,000\,\mathrm{kg/m^3}$ and $8\,000\,\mathrm{kg/m^3}$, respectively.

3.2. Short-range order around lead ions

3.2.1. Pb–O distances

For densities $\rho \leq 5\,970\,\mathrm{kg/m^3}$, the mean Pb–O distances, R, increase with increasing density, from 2.38 Å at $3\,000\,\mathrm{kg/m^3}$ to 2.42 Å at $5\,970\,\mathrm{kg/m^3}$ (Table 1). The σ^2 and β parameters only weakly depend on ρ, whereas the average co-ordination numbers increase from about 3.75 to 4.4. In densified glasses, however, the first

1. Relative deformation degree means the dispersion of tetraherda vertex positions around their ideal positions, normalised to the tetrahedron edge [52].

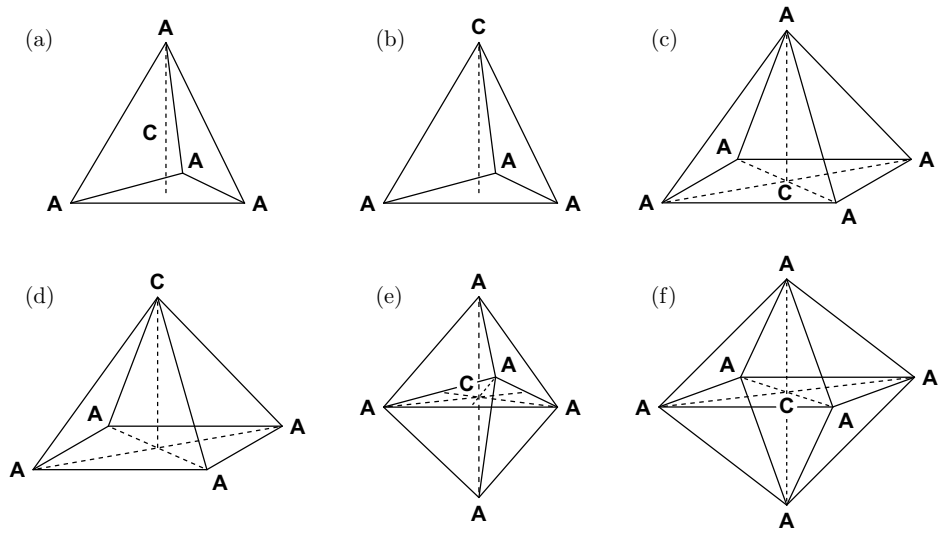

Figure 4. Structural units detected in the considered glasses;
C – cation (Si^{4+} or Pb^{2+}), **A** – anion (O^{2-})

Pb–O RDF peak can not be described by a single Γ-like function (3), and must be approximated using at least two such functions. The sub-peak shape parameters are practically the same for both of the densified samples we have simulated, but the associated co-ordination numbers are higher in the denser system (see Table 1). The peak splitting means that the Pb ions have a two-shell neighbourhood. The average Pb–O distances, R, for the two sub-shells are 2.40 Å and 2.75 Å.

3.2.2. Structural unit

The O–Pb–O angular distribution functions for several densities are shown in Figure 2. Although the presence of the 60° and 90° angles is readily seen, all the angles from 90° to 180° also appear in the sample. This suggests that the Pb atoms have a great variety of neighbourhoods.

The fraction of lead atoms co-ordinated with four oxygen atoms depends on the system's density and is significant only for $\rho < 5\,970\,\mathrm{kg/m^3}$ (Table 5). PbO_4 groups were identified as regular tetrahedra or square pyramids (Figure 4a and 4d). PbO_4 tetrahedra are dominant (at least 80% of all PbO_4 groups). The values of the tetrahedricity parameters T_1 and T_2 for PbO_4 tetrahedra are about 10 times higher than for SiO_4 tetrahedra. No clear dependence of the distribution of T_1 or T_2 values on density could be found. For all the densities, the distribution of T_1 and T_2 values correspond to the relative deformation degree, roughly equal to 20%, *i.e.* the PbO_4 tetrahedra are much less regular than the SiO_4 ones.

In order to characterise the PbO_4 groups of pyramid-like symmetry shown in Figure 4d (about 20% of all the PbO_4 groups), a shape estimator, P, was used [53], defined as:

$$P = \frac{\sum_i (l_{\mathrm{Pb-O},i} - l_{\mathrm{Pb-O}})^2}{l^2_{\mathrm{Pb-O}}} + \frac{\sum_i (l_{\mathrm{O-O},i} - l_{\mathrm{O-O}})^2}{l^2_{\mathrm{O-O}}}. \tag{6}$$

Table 3. The distribution of P-parameter values for PbO_4 groups at various glass densities

P parameter	0.0–0.2	0.2–0.4	0.4–0.6	0.6–0.8	>0.8
3 000 kg/m^3	48%	35%	2%	7%	8%
4 000 kg/m^3	46%	41%	4%	2%	7%
5 000 kg/m^3	58%	30%	3%	3%	6%
5 970 kg/m^3	66%	26%	6%	2%	—

Table 4. The structural parameters R, σ^2, β and N for Pb–Pb, Pb–Si, and Si–Si first peaks of radial distribution functions in $PbSiO_3$ glasses of various densities

ρ	Pb–Pb				Pb–Si				Si–Si			
[kg/m^3]	R [Å]	σ^2 [Å^2]	β	N	R [Å]	σ^2 [Å^2]	β	N	R [Å]	σ^2 [Å^2]	β	N
3 000	(I) 3.09	0.011	0.30	0.06	(I) 3.25	0.022	0.94	0.30	(I) 3.15	0.001	0.01	0.06
	(II) 3.49	0.032	0.634	1.36	(II) 3.63	0.034	0.02	3.50	(II) 3.28	0.003	0.001	1.99
	(III) 4.05	0.082	0.82	1.92								
4 000	(I) 3.09	0.010	0.01	0.04	(I) 3.30	0.023	0.40	0.51	(I) 3.16	0.001	0.01	0.06
	(II) 3.46	0.026	0.28	1.29	(II) 3.67	0.026	0.01	3.23	(II) 3.29	0.003	0.01	2.00
	(III) 4.07	0.097	1.02	1.83								
5 000					(I) 3.43	0.051	0.72	0.81	(I) 3.16	0.001	0.01	0.07
	(II) 3.46	0.031	0.10	1.72	(II) 3.65	0.029	0.04	3.21	(II) 3.29	0.003	0.02	2.02
	(III) 4.05	0.110	1.07	2.34								
5 970					(I) 3.38	0.025	0.30	1.82	(I) 3.13	0.005	0.03	0.08
	(II) 3.46	0.030	0.10	1.97	(II) 3.71	0.031	0.59	3.07	(II) 3.28	0.005	0.05	2.12
	(III) 4.04	0.090	0.92	2.86								
7 000					(I) 3.36	0.030	0.41	2.73	(I) 2.97	0.008	0.03	0.18
	(II) 3.41	0.030	0.11	2.27	(II) 3.76	0.067	0.91	3.48	(II) 3.29	0.011	0.25	2.75
	(III) 4.04	0.152	1.20	3.20								
8 000					(I) 3.28	0.027	0.09	2.81	(I) 2.97	0.012	0.03	0.57
	(II) 3.30	0.032	0.19	2.54	(II) 3.70	0.099	0.65	4.16	(II) 3.35	0.024	0.76	3.51
	(III) 3.95	0.153	1.25	3.48								

Table 5. The occurrence [%] of various PbO_n groups in the function of glass density

	PbO_3	PbO_4	PbO_5	PbO_6	other
3 000 kg/m^3	20.6%	51.6%	23.8%	3.0%	0.2%
4 000 kg/m^3	24.8%	55.4%	18.8%	0.4%	—
5 000 kg/m^3	6.0%	62.0%	26.4%	5.2%	0.4%
5 970 kg/m^3	0.2%	31.0%	45.6%	20.2%	2.4%
7 000 kg/m^3	—	6.0%	33.4%	43.6%	16.4%
8 000 kg/m^3	—	0.2%	7.8%	34.4%	57.6%

In Equation (6), $l_{\mathrm{Pb-O},i}$ is the length of the i^{th} Pb–O edge, and $l_{\mathrm{Pb-O}}$ is the average length of Pb–O edges, and similarly, $l_{\mathrm{O-O},i}$ is the length of the i^{th} O–O edge, and $l_{\mathrm{O-O}}$ is the average length of O–O edges. The distribution of the P values for pyramid-like PbO_4-groups is density-dependent: the pyramids are more regular at higher densities (see Table 3).

As stated above, only certain fractions of all the Pb atoms have four-fold oxygen co-ordination. Let us describe in brief other types of neighbourhoods of the lead atom.

In the low-density range ($\rho \leq 4\,000\,\mathrm{kg/m^3}$), 20%–25% of lead atoms have three-fold oxygen co-ordination and form roughly triangular pyramids (Figure 4b). In the same density range, about 20% of Pb atoms have five-fold co-ordination. Among the PbO_5 groups, distorted triangular bi-pyramids (more frequent) and square pyramids (less frequent) have been detected (Figures 4e and 4c, respectively). Several PbO_5 groups could not be classified.

The fraction of three-fold co-ordinated Pb atoms decreases with increasing density and is nil for $\rho > 5\,000\,\mathrm{kg/m^3}$. In rarefied glasses ($\rho \leq 5\,000\,\mathrm{kg/m^3}$), PbO_4 groups dominate. The Pb–O co-ordination number increases with increasing density. At normal density, five-fold oxygen co-ordinated lead atoms are most frequent, while PbO_6 groups dominate at $7\,000\,\mathrm{kg/m^3}$ and $8\,000\,\mathrm{kg/m^3}$. All the high-density structural units, with six-, seven-fold and higher co-ordination show poor symmetry and cannot be classified unambiguously.

4. Medium-range order

Let us consider in turn the second-neighbour RDFs (Section 4.1) and the cation-anion ring structure (Sections 4.2 and 4.3). The samples' homogeneity is briefly discussed in Section 4.4.

4.1. Si–Si, Pb–Si, and Pb–Pb radial correlations

4.1.1. Si–Si distances

It is impossible to reproduce the first Si–Si peaks with a single Γ-like function, as the peaks split into two sub-shells (see Table 4).

The first sub-peak (marked I in Table 4) is significant only for $\rho = 8\,000\,\mathrm{kg/m^3}$ (related co-ordination number about 0.6). The R values of the first sub-peak decrease from 3.15 Å to 2.97 Å, whereas those of the second sub-peak increase from 3.28 Å to 3.35 Å. For $\rho < 5\,970\,\mathrm{kg/m^3}$, the first Si–Si co-ordination number is stable (about 2.05–2.10), and increases from about 2.20 for $5\,970\,\mathrm{kg/m^3}$ to about 4 for $8\,000\,\mathrm{kg/m^3}$. The Si–Si distance closes a triangle, in which two edges are of the Si–O distance, and the Si–O–Si angles correspond to the ADF peak positions (Figure 2). Thus, the first Si–Si RDF peak is related to corner-sharing SiO_4 tetrahedra.

The Si–Si–Si angle distribution for $\rho \leq 5\,970\,\mathrm{kg/m^3}$ contains a single peak lying between 80° and 120° with its maximum at about 100°. At higher densities a rather sharp peak appears, with the maximum at 60°. Its presence is related to the existence of two-member Si–O–Si–O rings (see Section 4.2), corresponding to edge-sharing SiO_4 tetrahedra.

4.1.2. Pb–Pb distances

The first Pb–Pb peak splits into two main sub-peaks (marked II and III in Table 4), but at low densities a third sub-peak (I in the table) can be distinguished (see below). The R values of sub-peaks II and III decrease from 3.49 Å and 4.05 Å to 3.30 Å and 3.95 Å, respectively. The III sub-peak is significantly wider and more asymmetric than the II peak. An interpretation of these two sub-peaks is given in Section 4.3. The co-ordination numbers associated with the sub-peaks increase from about 1.4 to about 2.5 for the second peak, and from about 1.9 to about 3.5 for the third peak. This corresponds to an increase in the total average co-ordination number

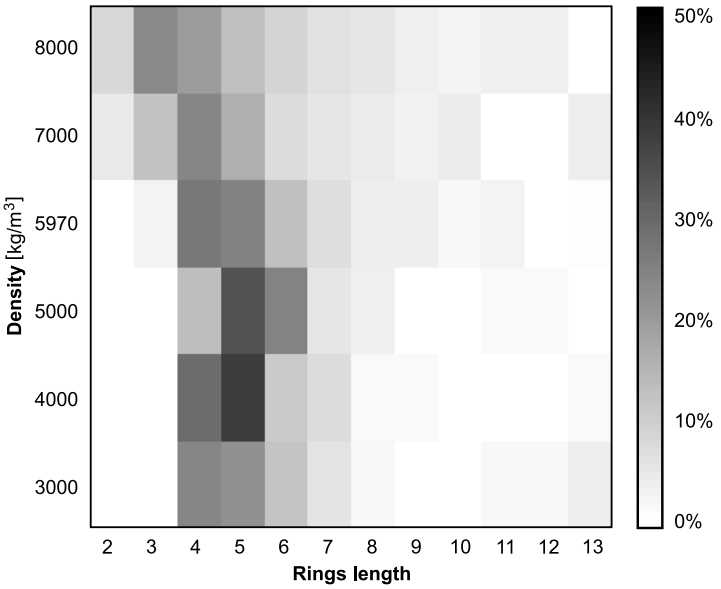

Figure 5. Distributions of the Si–O–Si–O–… rings' lengths in $PbSiO_3$ glasses of various densities

related to the first RDF maximum (composed of sub-peaks II and III) roughly from 3.3 to 6.

In the low density samples (the 3 000 kg/m^3 and 4 000 kg/m^3 runs), a pre-peak appears (I in Table 4) with $R = 3.09$ Å and very low related average co-ordination (about 0.05). Thus, there are very few so close Pb pairs within the simulation box.

The Pb–Pb–Pb angle distribution (Figure 2) contains two peaks, the first at about 60° and the second at about 110° for all densities.

4.1.3. Pb–Si distances

The first Pb–Si peak is also composite, and generally splits into two sub-peaks (Table 4). The first peak (I) has its R-values in the range from 3.25 Å to 3.43 Å, and the second peak (II) – in the range from 3.63 Å to 3.76 Å. The co-ordination numbers associated with sub-peak (I) increase from 0.3 to 2.8. The density dependence of the co-ordination numbers associated with sub-peak II is more complicated: they decrease from 3.5 Å for 3 000 kg/m^3 to 3.07 Å for the normal density, and then increase to 4.16 Å for 8 000 kg/m^3. This corresponds to an increase in the total co-ordination number related to the unresolved first RDF's peak from 3.8 to almost 7.

4.2. Si–O–Si–O–… rings

A closed chain of chemically bonded atoms, consisting of N cations and N anions is called an N-member ring. Below, we discuss the length statistics of linearly independent (basal) rings that span the full graph representing chemically bonded atoms. 2-member rings correspond to edge-sharing or face-sharing structural units. Since rings of lengths equal to 4, 5, 6, and 7 dominate in most of the "well relaxed" structural models of pure SiO_2, the 2-, 3- and 4-member rings are usually referred to as "strained" rings [54–58].

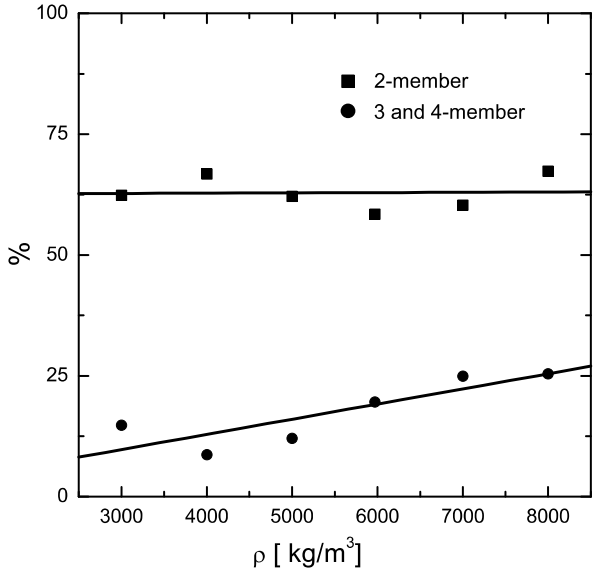

Figure 6. Distributions of the Pb–O–Pb–O–... rings' lengths in $PbSiO_3$ glasses of various densities

The connectivity graphs for Si and O ions have been calculated using an adjacency criterion with cut-off radii equal to 2.0 Å. Figure 5 shows the length distribution of Si–O–Si–O–... rings for all the considered densities.

A small fraction of 2-member rings, corresponding to edge-sharing SiO_4 tetrahedra, appears only in densified samples: 5% at 7 000 kg/m^3 and 8% at 8 000 kg/m^3. 3-member rings appear at and above the normal density (1% at normal density, 13% at 7 000 kg/m^3, 23% (dominating) at 8 000 kg/m^3). The share of 4-member rings ranges from 15% to 30% for the densities of 3 000–5 970 kg/m^3, and is about 20%–25% in densified glasses. Longer rings are present at all densities, and are less frequent than in pure silica.

4.3. Pb–O–Pb–O–... rings

The connectivity graphs for Pb and O ions have been calculated using an adjacency criterion with cut-off radii equal to 3.0 Å.

The fraction of 2-member rings weakly depends on the system's density and amounts to 60%–65% (Figure 6). In the density range of 3 000 kg/m^3–5 000 kg/m^3 the fraction of 3-member rings also remains almost constant (10%), while it increases to about 25% for higher densities. The remaining lead-oxygen rings are widely distributed at low densities (up to the length of 15). At higher densities, the rings' length does not exceed 8.

The Pb–O–Pb and O–Pb–O angles' distributions along the 2-member rings have been calculated. The distributions only weakly depend on the system's density, and generally become slightly wider with increasing density. Over 80% of all values of the Pb–O–Pb angles fall into the interval from 80° to 100°, for $\rho \leq 5\,970$, and the distributions are only 20° wide. For densified glass, the distribution is peaked in a slightly narrower interval, between 80° and 90°. The distribution of O–Pb–O

angles is more dispersed, but the peak maximum remains in the range from 80° to 90°, regardless of density. With increasing density the width of the O–Pb–O angular distribution increases from 70°–100° at 3 000 kg/m^3 to 50°–110° at 8 000 kg/m^3. Thus, for $\rho \leq 5\,970$ kg/m^3, the shape of 2-member lead-oxygen rings does not significantly depend on system density, and the Pb–O–Pb angles, having narrower distributions, are stiffer then the O–Pb–O angles.

The angular distributions along 2-member rings, described above, may now be compared with the corresponding distributions averaged over the whole simulation box (see Figure 2). The peaks in the range 75°–100° originate from the internal angles along 2-member rings, whereas other peaks and humps correspond to O–Pb–O and Pb–O–Pb angles, in which the oxygen and lead atoms belong to adjacent (node- or edge-sharing) rings.

In Section 4.1, the complex structure of the first Pb–Pb RDF has been described. It follows from the analysis of the lead-oxygen rings' geometry that the shorter Pb–Pb distances (peak II) originates from diagonal distances in 2-member Pb–O rings. The corresponding O–O diagonal distances contribute to wide RDFs' features between 3.3 Å and 3.6 Å (see Figure 1).

4.4. Sample homogeneity

In order to determinate whether the samples are spatially homogeneous or non-homogeneous, the standard χ^2-test has been used [59]. The whole simulation box was divided into n^3 cubic sub-cells, where n is the number of cells along the edge of the simulation box. If we mark the theoretical number of atoms in every sub-cell (*i.e.* the total number of atoms divided by the number of sub-cell) with $\bar{N}$, and the observed number of atoms in the i^{th} sub-cell – with N_i, then the random variable M,

$$M = \sum_i \frac{(N_i - \bar{N})^2}{\bar{N}^2}, \tag{7}$$

has an $\chi^2_{n^3-1}$ distribution, *i.e.* chi-square distribution with $s = n^3 - 1$ degrees of freedom:

$$\chi^2_s(x) = \int_0^x f_s(x')dx', \tag{8}$$

where

$$f_s(x) = \frac{x^{\frac{1}{2}(s-2)}}{2^{\frac{1}{2}s}\,\Gamma\left(\frac{1}{2}s\right)} \mathrm{e}^{-\frac{1}{2}x}, \tag{9}$$

and Γ is the Euler function. This implies that, if our sample is spatially homogeneous, the value of M has to be, with a fixed probability, less than a certain value q (quantile) of the $\chi^2_{n^3-1}$ distribution. A value of M superior to q means that the measured values have not been derived from the theoretical one, or that we have made a mistake with a probability equal to the so called level of significance α, $\alpha = \int_q^\infty f_s(x)dx$.

Three kinds of atoms were checked for the uniformity of their distribution: Pb and Si atoms separately, to obtain information about cation uniformity, and O atoms, to obtain information on the overall density distribution. Since the oxygen atoms are always in the first neighbourhood of lead or silicon atoms, it is possible to obtain

information about the connectivity of the whole simulated structure by performing the uniformity test for oxygen atoms only.

The results of the statistical tests for the samples' spatial uniformity can be summarised as follows. For $\rho \geq 5\,000\,\mathrm{kg/m^3}$, the distribution of all kinds of atoms in the simulation box is spatially uniform. For $\rho = 3\,000\,\mathrm{kg/m^3}$, with the level of significance not exceeding 0.01, the distributions of both silicon and lead atoms are non-uniform. The test for oxygen atoms has yielded almost 100% probability that the overall structure of $PbSiO_3$ glass is spatially non-uniform. Such a non-uniform structure also appears for $\rho = 4\,000\,\mathrm{kg/m^3}$, with the level of significance 0.3, but at the same time the hypothesis of non-uniformity of the spatial distribution of the other atoms is acceptable only at the level of 0.9.

5. Summary and comparison with the $PbGeO_3$ system

The structural results obtained for the $PbSiO_3$ system can be summarised as follows:

1. The short range ordering around silicon atoms changes slightly in the density range $3\,000$–$5\,970\,\mathrm{kg/m^3}$. Regular SiO_4 units dominate in the SiO_2 subsystem for this range. In densified structures some SiO_4 pyramid-like structures have been detected. In the most densified glass ($8\,000\,\mathrm{kg/m^3}$), SiO_5 triangular bi-pyramids and square pyramids are dominating.
2. The PbO subsystem has a much more complex structure. Among PbO_4 structural units (identification cut-off radius of 3.0 Å), both regular tetrahedra (80% of PbO_4) and regular square pyramids (20% of PbO_4) have been detected. The tetrahedra are more regular at lower densities. However, with increasing density the contribution of 4-co-ordinated lead ions decreases, and the fraction of lead atoms with five- and six-fold oxygen co-ordination becomes significant. PbO_5 groups appear in two quite well-defined forms: square pyramids with the oxygen atoms in the corners and the Pb atom in the centre of the oxygen basal square (or slightly above this point), and triangular bi-pyramids (Figures 4c and 4e). PbO_6 and PbO_7 groups show poor symmetry and could not be classified.
3. The medium-range order is subject to remarkable changes. 4-, 5- and 6-member Si–O rings dominate for $\rho \leq 5\,970\,\mathrm{kg/m^3}$. With increasing density, the number of shorter, strained rings increases significantly. In highly rarefied glasses, in contradistinction to the normal- and high-density phases, Si–O rings shorter than 4 are absent.
4. The highly rarefied $PbSiO_3$ glass has a spatially non-uniform (porous) structure. For $\rho = 3\,000\,\mathrm{kg/m^3}$, with the significance level of about 0.01, distributions of both silicate and lead atoms are non-uniform.

The results of similar MD simulations of the structure of lead-germanate glass, $PbGeO_3$, for the same densities, have been described in detail in [23]. Let us now compare them with the present results for $PbSiO_3$ glasses.

1. The short-range ordering around silicon atoms (SiO_4 tetrahedra) remains unaffected by density variations in the range $3\,000$–$5\,000\,\mathrm{kg/m^3}$, whereas in germanate glasses Ge atoms have a stable neighbourhood (GeO_4 tetrahedra)

in a wider density range, 3 000–8 000 kg/m^3. In general, the SiO_4 tetrahedra are slightly more regular than the GeO_4 ones. In densified silicate glasses, some SiO_5 groups appear. At the highest density simulated (8 000 kg/m^3) such structural units dominate, while some SiO_6 groups appear as well. The latter have been recognised as square bi-pyramids. In the germanate samples, only GeO_4 tetrahedra were present in the whole density range.

2. The Pb atom neighbourhood in $PbGeO_3$ glasses is structurally very similar to that described above for $PbSiO_3$ glasses. This is the case in the whole considered range of densities.
3. In rarefied $PbGeO_3$ samples, the Ge–O rings longer than 8 are absent, but there exist some short Ge–O rings. In $PbSiO_3$ glass, the situation is quite different: short rings (shorter than 4) are absent and some very long rings are present.
4. Both $PbSiO_3$ and $PbGeO_3$ have evidently spatially non-uniform (porous) structure (with the significance level of about 0.01) at $\rho = 3\,000$ kg/m^3. However, the $PbGeO_3$ glass is still pretty non-uniform at $\rho = 4\,000$ kg/m^3 (with the significance level of 0.01), while in the $PbSiO_3$ system the non-uniformity hypothesis can be accepted only at a significance level of about 0.30. The hypothesis of non-uniformity of the spatial distribution of the silicon and lead atoms (for $PbSiO_3$) for $\rho = 4\,000$ kg/m^3 is acceptable only at the level of significance of 0.90, and that of germanium and lead (for $PbGeO_3$) – at the significance level of about 0.3.

6. Concluding remarks

In this paper, we have presented the results of extensive MD simulations of $PbSiO_3$ glasses in the density range from 3 000 kg/m^3 to 8 000 kg/m^3. As mentioned in Section 2 above, the obtained glasses are stable for $\rho \leq 5\,970$ kg/m^3 (*i.e.* they maintain their densities during the zero external pressure simulations). The existence of stable low-density $PbSiO_3$ glass is documented in [37]. The simulated densified $PbSiO_3$ expand continuously to roughly normal density with the constant volume restriction removed, so the presented results correspond to non-equilibrium pressure-induced structures. In order to analyse the short-range order, we have introduced a couple of new shape estimators of basis structural units. The medium-range order has been characterised in terms of basal cation-anion rings. In particular, the ring length statistics and ring geometry have been taken into account (angular distributions along rings of a given length). We have shown, that our new methods of structural analysis allow a detailed structural description and can be used to recognise trends in the structural changes related to variations of glass density.

Acknowledgements

The work has been partially sponsored by KBN, under grants 7 T11F 013 21 and 4 T11F 019 25. The opportunity to perform our simulations at the TASK Computer Centre in Gdansk, Poland, is kindly acknowledged.

Appendix A: Basic structural data at normal density

Table A1. A comparison of the experimental and MD-simulated inter-atomic distances and co-ordination numbers (in square brackets) for $PbSiO_3$ glass at its normal density (5 970 kg/m^3); (a) – ref. [60]; (b) – ref. [61]; (c) – ref. [62]; (d) – ref. [63]; (e) – ref. [22]

Glass composition	Atom pair	experiments	MD simulations (e)
x =0.3–0.5	Pb–O	2.2–2.3 Å, 2.45–2.6 Å (a)	2.3 Å
x = 0.5	Pb–O	2.25 Å, 2.45 Å (b)	2.3 Å
x = 0.67	Pb–O	2.35 Å [4.3] (c)	2.3 Å [4.7]
x = 0.33	Si–O	1.615 Å [3.92] (d)	1.64 Å [4.1]
x = 0.5	Si–O	1.625 Å [3.92] (d)	1.64 Å [4.1]
x = 0.67	Si–O	1.62 Å (b), 1.6 Å [3.8] (c), 1.63 Å (d)	1.62 Å [4.1]

Appendix B: Outline of the ring perception algorithm

Let us present the ring determination method in more detail. The atomic system is represented as an undirected, simple graph, with each atom associated with a node and each bond between two atoms associated with an edge joining the respective nodes. Thus, groups of chemically bonded atoms in the system correspond to rings (cycles, loops) in the graph. Hence, the problem is reduced to the rings' determination. Recently, Balducci and Pearlman [64] have presented an exact and efficient algorithm for the determination of a minimum basis (the smallest set of smallest rings, or SSSR) of the ring space of a structure. In [64], a communication network analogy is developed. "Path-messages" convey information on their way through the network, and propagate by means of transceivers and communication channels during alternate, synchronous "send" and "receive" states of the network. The rings' perception *i.e.* SSSR identification, is carried out by classifying the path-messages' collisions on a common receiver.

Our new approach, called *pre-filtering* [65, 66], has been designed and implemented to handle and eliminate redundant information processing when selecting rings to enter an SSSR, *i.e.* to feed no duplicated information to the linear independence test on rings, and thus reduce calls to the most demanding procedure in terms of computational order. The efficiency of a perfect hashing algorithm is actually met by the *pre-filtering* method.

Basic definitions

- An edge sequence of length (size) $L-1$ in a graph is a finite sequence of edges $(i_1,i_2),(i_2,i_3),\ldots,(i_{L-1},i_L)$, wherein each edge is denoted by the pair of nodes it connects; if $i_1 = i_L$ or $i_1 \neq i_L$, the edge sequence is closed or open respectively.
- An edge sequence of distinct edges constitutes an edge train.
- An open edge train in which all nodes are distinct is called a path.
- A closed edge train in which all nodes are distinct is called a ring.
- The symmetric difference, or ring sum, or linear combination of two rings, A and B, is defined as $A \oplus B = (A \cup B) \backslash (A \cap B)$.

Process overview

Graphs considered are simple, finite and undirected; although not strictly necessary, they are furthermore supposed to be connected, so that they contain $R = E - N + 1$ linearly independent rings, where E and N are the numbers of edges and nodes, respectively.

Given a graph containing N nodes and E edges, representing the system, two main tasks are performed: identification of a superset of a minimal basis of rings, and selection of a set of $R = E - N + 1$ rings to form an SSSR.

The graph is considered as a synchronous communication network associating each node to a transceiver, each edge to a communication channel, and each path to a "path-message". All transceivers, during alternating send/receive cycles, simultaneously propagate path-messages through

the communication channels linking adjacent nodes in such a way that any message originating from a node m and received by a node n is forwarded to all nodes connected to n but m.

The entire process is such that, at any stage, all path-messages are of the same length, this length being increased each time messages are retransmitted, so that rings are identified and processed in the increasing length order to build up an SSSR.

Basically, the whole process consists of four phases:

1. communication network initialisation;
2. path-messages sending;
3. path-messages receiving;
4. rings selection,

and develops cycling over 2 through 4 until an SSSR is obtained.

Once a ring has been identified, it must undergo a linear independence test against the elements of the SSSR determined so far in order to be entered or discarded. As clearly follows from the detailed description of the algorithm given in [64] a ring of length L may, in principle, be built as many as L times (once per component node). Thus, the same L-sized ring may be submitted up to L times to the linear independence test.

Balducci and Pearlman proposed to use the well-known "hashing" [67] method to avoid multiple linear independence tests on the same ring. Assuming the choice a suitable hashing function and a suitably dimensioned hash table associated with it, the method approaches a perfect hashing algorithm.

A new method (*pre-filtering*) is now presented to substitute hashing, ensuring that each ring is checked for linear independence exactly once.

Let us briefly anticipate how rings are built up from path-messages collisions. Think of path-messages as messages describing the time evolution of paths through the communication network and define a collision of paths' messages as their arrival on the same transceiver at the same time. As mentioned above, the communication network operations are driven in such a way, that at any stage all the path-messages are of the same length, be it L.

It is easily seen that the union of two entirely separate (both edge-disjoint and node-disjoint) path-messages – save for their first edge, traversed in opposite directions – colliding at a node n, gives a ring of length $2L-1$, while the union of two entirely separate path-messages – save their first node – closing on a node n, gives a ring of length $2L$. Paths coupling to form rings will be referred to as the ring identification process.

Upward selection

The formation of a ring by collision on all of its nodes will be referred to as full formation. The appearance of full formation in the communication network depends on how paths messages are propagated.

Full formation suggests how to devise a strategy to send the independence test to no more than one L-sized ring out of the L possible equal ones.

Using an arbitrary numbering for nodes, let us suppose that full formation is enforced and all the rings closing on node 1 have been processed. When operating on node 2, all rings closing on it after passing through node 1 may be safely ignored, since they have already been identified while processing node 1. Generally, having processed the rings closing on nodes $1,\ldots,n-1$, all rings containing a node $m<n$ can be ignored while processing node n; in other words, only the rings originating from nodes numbered higher than n are taken into account, thus operating an *upward selection*.

Obviously *full formation* requires all path-messages originating from a common source and colliding at any node of degree >2 to be propagated further.

Although sufficient, *full formation* of all rings is not a necessary requisite for *upward selection* since, for rings that can be expressed as a linear combination of the identified elements of the SSSR, being also identified from collisions at each of their nodes is irrelevant. As a general result, with regards to *upward selection*, it is sufficient to propagate just one *path-message* out of all the distinct ones sharing a common origin and colliding on the same node of degree >2 [68].

Inner-node intersection

Let us define an *inner-node intersection* of two edge-disjoint paths closing on a common node as a passage through a common node other than the first, if any, and the last. A union of any two L-sized *inner-node intersecting* paths originating from a common node m and closing on a node n is a linear combination of two or more rings shorter than $2L$. Thus, path pairs showing an inner-node intersection can be safely ignored during the rings identification process.

Inner-edge intersection

Let us define an *inner-edge intersection* of two paths closing on a common node as an intersection on an edge other than the first one, if any, traversed in opposite directions. Generally, a union of any two L-sized *inner-edge intersecting* paths originating from a common node m and closing on a node n contains two or more rings shorter than $2L$, but is neither a ring nor a linear combination of rings.

Collapsed path

An edge sequence traversing a node more than once will be referred to as a collapsed path. A union of two paths of which at least one is collapsed, sharing a common origin and closing on a common node, determines an *inner node-intersection* and/or an *inner edge-intersection*. Path collapse can easily be prevented while propagating path-messages.

The combined use of *upward selection*, pairing of paths showing no *inner-node/inner-edge intersection* when building rings to send the linear independence test, together with the prevention of *path-message collapse*, constitutes *pre-filtering*: it ensures by its construction that no ring is tested for linear independence more than once.

References

[1] Wang C C 1970 *Phys. Rev.* **B 2** 2045
[2] Wiza J L 1979 *Nucl. Instrum. Meth.* **62** 587
[3] Trzebiatowski K, Murawski L, Kościelska B, Chybicki M, Gzowski O and Davoli I 1997 *Proc. Conf. on Fundamentals of Glass Science and Technology*, June 9–12 1997, Växjö, Sweden
[4] Warrel C A and Henshall T 1978 *J. Non-Cryst. Solids* **29** 283
[5] Verweij H and Konijnendijk W L 1976 *J. Am. Ceram. Soc.* **11−12** 517
[6] Zahra A M and Zahra C Y 1993 *J. Non-Cryst. Solids* **155** 45
[7] Fayon F, Bessada C, Massiot D, Farnan I and Coutures J P 1998 *J. Non-Cryst. Solids* **232−234** 403
[8] Fayon F, Landron C, Sakurai K, Bessada C and Massiot D 1999 *J. Non-Cryst. Solids* **243** 39
[9] Wang P W and Zhang L 1996 *J. Non-Cryst. Solids* **194** 129
[10] Morikawa H, Takagi Y and Ohno H 1982 *J. Non-Cryst. Solids* **53** 173
[11] Imaoka M, Hasegawa H and Yasui I 1986 *J. Non-Cryst. Solids* **85** 393
[12] Yamada K, Matsumoto A, Niimura N, Fukunaga T, Hayashi N and Watanabe N 1986 *J. Phys. Soc. Jap.* **55** 831
[13] Suzuya K, Price D L, Saboungi M-L and Ohno H 1997 *Nucl. Inst. Meth. Phys. Res.* **B133** 57
[14] Masteraro V R, Zanotto E D, Lequeux N and Cortès R 2000 *J. Non-Cryst. Solids* **262** 191
[15] Witkowska A, Rybicki J, Trzebiatowski K, Di Cicco A and Minicucci M 1999 *Proc. 5^{th} Int. Conf. on Intermolecular Interactions in Matter*, Lublin, Poland, pp. 42–47
[16] Witkowska A, Rybicki J, Trzebiatowski K, Di Cicco A and Minicucci M 2000 *J. Non-Cryst. Solids* **276** 19
[17] Rybicki J, Rybicka A, Witkowska A, Bergmański G, Di Cicco A, Minicucci M and Mancini G 2001 *J. Phys. CM* **13** 9781
[18] Damodaran K V, Rao B G and Rao K J 1990 *Phys. Chem. Glasses* **31** 212
[19] Cormier G, Peres T and Capobianco J A 1996 *J. Non-Cryst. Solids* **195** 125
[20] Rybicki J, Alda W, Rybicka A and Feliziani S 1996 *Comp. Phys. Commun.* **97** 191
[21] Rybicka A, Chybicki M, Laskowski R, Alda W and Feliziani S 1997 *Proc. 4^{th} Int. Conf. on Intermolecular Interaction in Matter*, Gdansk, Poland, p. 42
[22] Rybicka A 1999 *The Structure and Properties of Lead-silicate and Lead-germanate Glasses: a Molecular Dynamics Study*, PhD Thesis, Gdansk University of Technology, Gdansk (in Polish)

[23] Rybicka A, Rybicki J, Witkowska A, Feliziani S and Mancini G 1999 *Comput. Met. Sci. Tech.* **5** 67
[24] Rajiv W J, Kalia K, Vashishta P and Rino J P 1994 *Phys. Rev.* **B 50** 118
[25] Olivi-Tran N and Jullien R 1995 *Phys. Rev.* **B 52** 258
[26] Valle R G D and Venuti E 1996 *Phys. Rev.* **B 54** 3809
[27] Rat E, Foret M, Courtens E, Vacher R and Arai M 1999 *Phys. Rev. Lett.* **83** 1355
[28] Vacher R, Courtens E, Foret M, Hehlen B, Rat E, Casalta H and Dorner B 2000 *Physica* **B 276–278** 427
[29] Ishikawa K, Uchiyama Y, Ogawa H and Fujimura S 1997 *Appl. Surf. Sci.* **117–118** 212
[30] Zhu D M and Weng H F 1995 *J. Non-Cryst. Solids* **185** 262
[31] Woignier T, Duffours L and Phalippou J 1996 *J. Non-Cryst. Solids* **194** 283
[32] Hiramatsu A, Arai M, Shibazaki H, Tsunekawa M, Otomo T, Hannon A C and Bennington S M 1996 *Physica* **B 219–220** 287
[33] Vogel E M, Grabow M H and Martin S W 1996 *J. Non-Cryst. Solids* **204** 95
[34] Tan C Z, Arndt J and Xie H S 1998 *Physica* **B 252** 28
[35] Tan C Z and Arndt J 1999 *J. Non-Cryst. Solids* **249** 47
[36] Inamura Y, Arai M, Nakamura M, Otomo T, Kitamura N, Bennington S M Hannon A C and Buchenau U 2001 *J. Non-Cryst. Solids* **293–295** 389
[37] Rigato V, Boscarino D, Maggioni G, Mariotto G, Pivin J C and Della Mea G 1996 *Nuc. Inst. Meth. Phys. Res.* **B 116** 424
[38] Hockney R W and Eastwood J W 1987 *Computer Simulation using Particles*, McGraw-Hill
[39] Rapaport D C 1995 *Art of the Molecular Dynamics Simulation*, University Press, Cambridge
[40] Brostow W, Chybicki M, Laskowski R and Rybicki J 1998 *Phys. Rev.* **B 57** 13448
[41] Laskowski R, Rybicki J and Chybicki M 1997 *TASK Quart.* **1** 96
[42] Laskowski R 2000 *TASK Quart.* **4** 531
[43] Rybicki J, Laskowski R and Feliziani S 1996 *Comp. Phys. Comm.* **97** 185
[44] Bergmański G, Rybicki J and Mancini G 2000 *TASK Quart.* **4** 555
[45] Rybicki J, Bergmański G and Mancini G 2001 *J. Non-Cryst. Solids* **293–295** 758
[46] http://www.task.gda.pl/software
[47] Filipponi A 1994 *J. Phys. CM* **6** 8415
[48] D'Angelo P, Di Nola A, Filipponi A, Pavel N V and Roccatano D 1994 *J. Chem. Phys.* **100** 985
[49] Filipponi A and Di Cicco A 1995 *Phys. Rev.* **B 51** 12322
[50] Medvedev N N and Naberukhin Y I 1987 *J. Non-Cryst. Solids* **94** 402
[51] Rybicki J, Witkowska A, Bergmański G, Bośko J, Mancini G and Feliziani S 2001 *Comput. Met. Sci. Tech.* **7** (1) 91
[52] Bergmański G, Białoskórski M, Rybicki J and Rychcik-Leyk M 2004 *Comput. Met. Sci. Tech.* (submitted)
[53] Rybicki J, Witkowska A and Bosko J 2000 *Optica Applicata* **30** (4) 701
[54] Rino J P, Ebbsjo I, Kalia R K, Nakano A and Vashishta P 1993 *Phys. Rev.* **B 47** 3053
[55] Wei Jin, Kalia R K, Vashishta P and Rino J P 1994 *Phys. Rev.* **B 50** 118
[56] Elliott R 1995 *J. Non-Cryst. Solids* **182** 1
[57] Hamann D R 1997 *Phys. Rev.* **B 55** 14784
[58] Roder A, Kob W and Binder K 2001 *J. Chem. Phys.* **114** 7602
[59] Massey F J Jr 1951 *J. Am. Sta. Assoc.* **46** 70
[60] Verweij H and Konijnendijk W L *J. Am. Ceram. Soc.* **11–12** 517
[61] Imaoka M, Hasegawa H and Yasui I 1986 *J. Non-Cryst. Solids* **85** 393
[62] Morikawa H, Takagi Y and Ohno H 1982 *J. Non-Cryst. Solids* **53** 173
[63] Yamada K, Matsumoto A, Niimura N, Fukunaga T, Hayashi N and Watanabe N 1986 *J. Phys. Soc. Jap.* **55** 831
[64] Balducci R and Pearlman R S 1994 *J. Chem. Inf. Comput. Sci.* **34** 822
[65] Mancini G 1997 *TASK Quart.* **1** 89
[66] Mancini G 2002 *Comp. Phys. Commun.* **143** 187
[67] Knuth D E 1990 *Sorting and Searching, The Art of Computer Programming*, Vol. 3, Addison-Wesley, Reading, MA
[68] Horton J D 1987 *SIAM J. Comput.* **16** 358